Hindawi
International Journal of Antennas and Propagation
Volume 2023, Article ID 2788309, 12 pages
https://doi.org/10.1155/2023/2788309

Research Article

A Conformal Phased Array with Low Profile and Wide-Scanning Performance for SAR Application

Runzhi Tang, Senlin Lu, Shiwei Qu, and Shiwen Yang

School of Electronic Science and Engineering, University of Electronic Science and Technology of China (UESTC), Chengdu, China

Correspondence should be addressed to Shiwei Qu; shiweiqu@uestc.edu.cn

Received 28 August 2023; Revised 12 November 2023; Accepted 16 December 2023; Published 28 December 2023

Academic Editor: Shobhit K. Patel

A low-profile wide-scanning conformal phased array (CPA), with cavity-backed stacked patch elements, is presented in this paper. To reduce the array profile, a partially dielectric-filled cavity is employed in each element, and to enhance its scanning performance, the cavity walls are deliberately modified. Finally, the designed element operates in a frequency band of 1.45~1.75 GHz, with a profile of 0.086 λ_h (λ_h is the free-space wavelength at 1.75 GHz), and achieves ±60° scanning in the *E*/*H*-planes, with the reflection coefficient below −7 dB. The proposed design method and all numerical results are experimentally verified by a 4 × 4 CPA prototype.

1. Introduction

Synthetic aperture radars (SARs) are widely applied for high-resolution imaging in ground target reconnaissance and surveillance [1, 2]. This requires antennas to possess fast and flexible multibeam scanning capabilities. In these systems, fixed-beam antennas support directional radiation [3] but lack the ability for beam scanning. Mechanically scanned antennas enable scanning by mechanical rotation [4], but it is challenging to generate freely controlled multiple beams. Comparatively, phased arrays can overcome these limitations [5, 6] and exhibit superior suitability for SAR applications. As illustrated in Figure 1(a), the SAR equipped with a phased array allows simultaneous observation of multiple targets on multiple swathes during motion.

However, conventional planar configurations severely restrict the applications of phased arrays on the curved platforms with limited space, such as the SAR pod shown in Figure 1(b). Therefore, conformal phased arrays (CPAs) [7–9] have gained increased attention due to their lower aerodynamic drag and lower radar cross-section. They have become optimal solutions on high-speed platforms such as aircraft and ships [10, 11].

Endfire arrays are easily conformable and have a low profile, but they are commonly applied to scan in the horizontal plane and detect airborne targets [12]. However, the CPAs are required to scan in lower half-space to gaze at ground targets in SAR applications. Therefore, considering that the SAR pods are cylindrical, the CPAs with broadside radiation capability are more suitable for these application requirements. Moreover, according to the authors in reference [13], the arrays need to possess a wide-angle scanning capability to achieve higher resolution by steering the beam in a wide-angle range to always focus on the targets.

Flexible materials, e.g., polyimide film (PIF), can be easily conformed to the surface of the platform, making them suitable for designing conformal antennas. Over the past decade, some conformal antennas based on the PIF are reported [14, 15]. For example, a monopole antenna is presented in reference [14], which exhibits insensitivity of impedance matching and radiation pattern to the bending of the PIF. However, the bending effect is not verified in arrays. In reference [15], the authors proposed a linear CPA that is easily conformed to an unmanned aerial vehicle due to the flexibility of PIF; however, its scanning performance is limited in the *E*-plane.

Recently, substrate-integrated waveguide (SIW) slot arrays are broadly reported because of their low cost and low profile [16–18]. However, limited by the feeding mechanism of SIW, the scanning ability of the array is limited to only

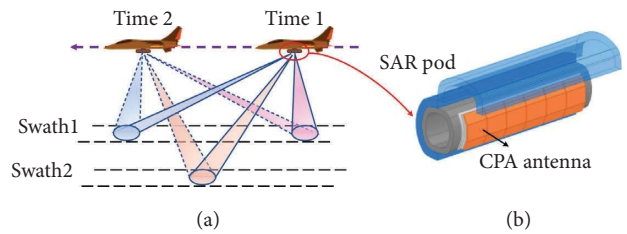

FIGURE 1: (a) Schematic diagram of SAR application. (b) SAR pod with CPA.

one plane [17, 18]. Meanwhile, a linear CPA with a low profile is proposed by the authors in reference [19], which conforms to a wing of the airframe, and achieves a wide-scanning range of ±70° but only in the *E*-plane.

Additionally, microstrip antennas are also widely used in conformal array designs, due to their simple structure and low profile [20–22]. In reference [21], a cavity-backed conformal array is proposed and obtains broadband operation while keeping a low profile. However, the beam scanning is realized by switching the excitations to different subarrays in the whole array, instead of in a phased manner. In reference [22], a CPA with microstrip Yagi elements is proposed, which achieves a low profile and 2D beam steering ability, but only within an extremely narrow band around 20.7 GHz.

In this paper, a low-profile wide-scanning CPA is proposed based on the cavity-backed stacked patch element. The cavity is modified to improve the interelement isolation and subsequently the scanning performance of the element. The designed element features a low profile of 0.086 λ_h (λ_h is the free-space wavelength at 1.75 GHz), while achieving a relatively wide fractional bandwidth of 18.75%, i.e., 1.45~1.75 GHz, as well as a wide-scanning range of ±60° in the *E*/*H*-planes. To verify the validity of this design method, a 4 × 4 CPA prototype is manufactured and measured.

2. Element Design

The evolution of the designed element is illustrated in Figure 2. Initially, a stacked patch element with a backed cavity is designed, as shown by antenna 1 in Figure 2(a). To enhance the interelement isolation and consequently improve the scanning performance, the cavity side walls in antenna 2 are extended, as shown in Figure 2(b). Furthermore, to improve impedance matching when scanning in the *H*-plane (XOZ plane), eight notches are cut on the cavity side walls of antenna 3, i.e., the proposed element, as shown in Figure 2(c). Note that, the lower part of the cavity wall is replaced by a series of via holes for ease of manufacturing.

Figure 3 shows the detailed geometries of the proposed element with overall sizes of $0.484 \times 0.496 \times 0.086\ \lambda_h^3$. It is composed of three components, i.e., two stacked patches, a feedline, and a modified cavity. As shown in the figure, the upper patch is printed on the top surface of substrate 1 with a thickness of $h_1 = 1$ mm and a relative permittivity of $\varepsilon_r = 2.2$, whereas the lower patch is on the top side of the substrate 2 (thickness $h_2 = 2$ mm and $\varepsilon_r = 2.2$). The fork-shaped microstrip feedline is printed on substrate 3 (thickness $h_3 = 0.8$ mm and $\varepsilon_r = 2.2$), which is to be connected to a 50-Ω coaxial connector. Meanwhile, the abovementioned arrangement ensures that an optimal amount of electromagnetic power is coupled from the lower patch to the upper one, thus providing wideband operation. Finally, the cavity is formed by both the aluminum walls and a series of via holes, while being partially filled with a high-permittivity dielectric, i.e., substrate 4 (thickness $h_4 = 3$ mm and $\varepsilon_r = 4.4$), to achieve a lower profile.

As shown in Figure 4, the reflection coefficient of the three antennas is simulated in an infinite array environment. Compared to antenna 1, the reflection coefficient of antenna 2 decreases from approximately −7 dB to below −10 dB when scanning at 60° in the *E*-plane (YOZ plane) with the assistance of the extended cavity wall but significantly deteriorates when scanning in the *H*-plane. In contrast, antenna 3 with a modified cavity effectively resolves this issue. The results reveal that the reflection coefficient of antenna 3 is improved from −6 dB to −7 dB in the operating band, i.e., 1.45~1.75 GHz, when scanning at 60° in the *H*-plane, while maintaining a low reflection coefficient in the *E*-plane scanning case.

To illustrate the operating principle of the modified cavity, Figure 5 shows the current and electric-field distributions on the top surface of the upper patch and cavity walls of antennas 2 and 3, when scanning at 60° in the *H*-plane at 1.7 GHz. According to the authors in reference [23], although the extended cavity walls are beneficial to *E*-plane scanning, strong coupling currents also arise on the cavity walls parallel to the *Y*-axis, as shown in Figure 5(a). Meanwhile, strong electric fields accumulate in the areas marked by black frames in Figure 5(c), indicating a relatively strong *H*-plane element coupling. This negative coupling subsequently deteriorates the impedance matching when scanning in the *H*-plane. To address this problem, similar to that in [23], the parts of the cavity wall with strong coupling currents are cut, leading to the suppression of the negative strong electric fields, as shown in Figures 5(c) and 5(d). Therefore, a better impedance matching in the *H*-plane 60° scanning case is achieved, as presented in Figure 4(b). Since the modified cavity still maintains the effective interelement isolation along the *E*-plane, the impedance matching when scanning in the *E*-plane remains acceptable.

Additionally, the key parameters of the proposed element are studied. As shown in Figure 6, the reflection coefficient when scanning in *E*/*H*-planes can be optimized by increasing the width w_1 and depth h_6 of the wall notches. As a compromise of lower reflection coefficient and structural stability, w_1 and h_6 are optimized to be 30 mm and 6.5 mm, respectively, with the inner dimensions of 77×77 mm^2.

3. Experiment of the Conformal Array

To verify the feasibility of the design method, a 4 × 4 CPA prototype based on the proposed element is manufactured and assembled. It is mounted on a polyhedral platform, as shown in Figure 7, and a larger-scale array can be constructed for the practical applications by arranging more

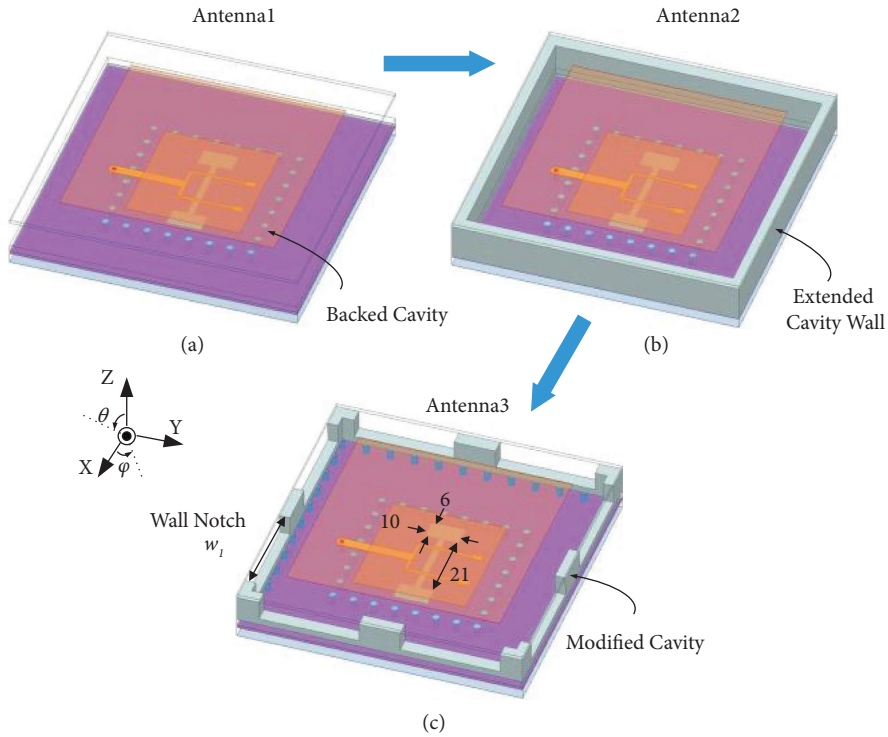

FIGURE 2: Evolution of the proposed element. (a) Antenna 1, with the unmodified cavity. (b) Antenna 2, whose cavity side walls are extended. (c) Antenna 3, with the modified cavity. Key parameter: $w_1 = 30$ mm.

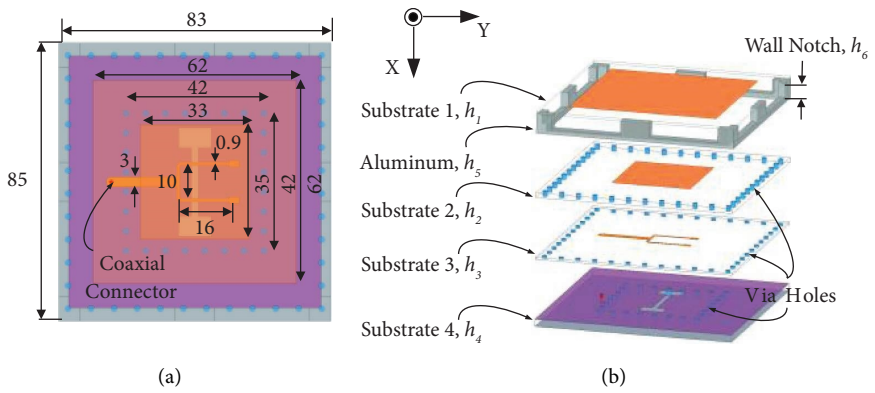

FIGURE 3: Element geometries. (a) Top view of the element. (b) Exploded views of elements. Key parameters: $h_1 = 1$, $h_2 = 2$, $h_3 = 0.8$, $h_4 = 3$, $h_5 = 8$, and $h_6 = 6.5$ (in mm).

4×4 CPA subarrays along the longitudinal direction of the SAR pod. The physical aperture dimensions of the CPA are $328 \times 352\ \text{mm}^2$, including a 10 mm extension of the ground along the E-plane for fixing purposes. Since the surface of the practical platform is cylindrical with a large radius, the edge elements of the array must be bent by 20° to fulfill the conformal requirement. Additionally, the polymethacrylimide (PMI) foam is utilized between the lower and the upper patch layers to support the substrates.

The array beam facilitates flexible scanning by controlling the excitation phase of each element. The authors in reference [24] present a detailed derivation of the excitation phase formula for general CPAs. As an example, in the H-plane scanning case, the excitation phase of the four elements in the cross-sections shown in Figure 7(d) can be expressed as

$$\Phi_i = -k_0 \left(x_i \sin\theta + z_i \cos\theta\right), \tag{1}$$

where $i = 1$ to 4, k_0 is the wavenumber in the free space, x_i and z_i are the coordinate positions of elements in the Cartesian coordinate system in Figure 7(d), and θ is the scanning angle. It is noteworthy that the excitation amplitudes are equal for all elements.

Since the scale of the 4×4 array is not large enough, the impedance matching of each element slightly differs from the others. To illustrate the impedance matching condition of the array, the measured and simulated active reflection

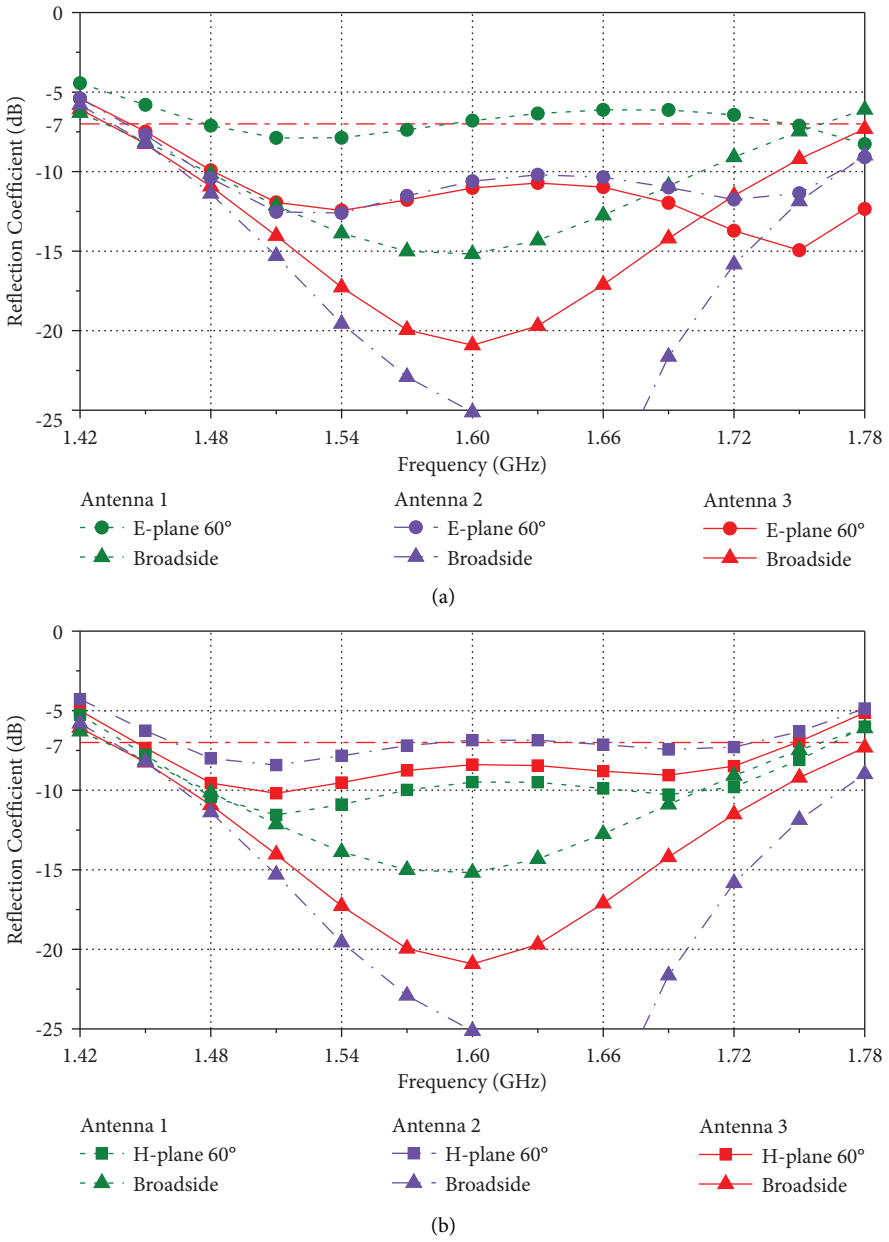

Figure 4: Simulated reflection coefficient of the antennas 1, 2, and 3, when scanning in the (a) *E*-plane and (b) *H*-plane.

coefficients of element 4, as a typical element, are shown in Figure 8. The measured active reflection coefficient can be calculated by using the following equation:

$$\text{Active } S_m = \sum_{n=1}^{N} \left(\frac{a_n}{a_m}\right) S_{mn}, \tag{2}$$

where $m = 4$, N is the number of elements, a_m and a_n are the corresponding excitations determined by the scanning angles, and S_{mn} is the measured passive S-parameter.

As shown in Figure 8, throughout most of the operating band, i.e., 1.45~1.75 GHz, the simulated active reflection coefficients of the typical element are lower than −7 dB when scanning within ±60° in the *E*-plane, and below −10 dB in the *H*-plane. The measured reflection coefficients exhibit slight discrepancies from the simulated ones; however, they demonstrate good overall agreement. These discrepancies are mainly caused by assembly errors, especially the misalignment of the inner core of the coaxial connector in the via hole of ground.

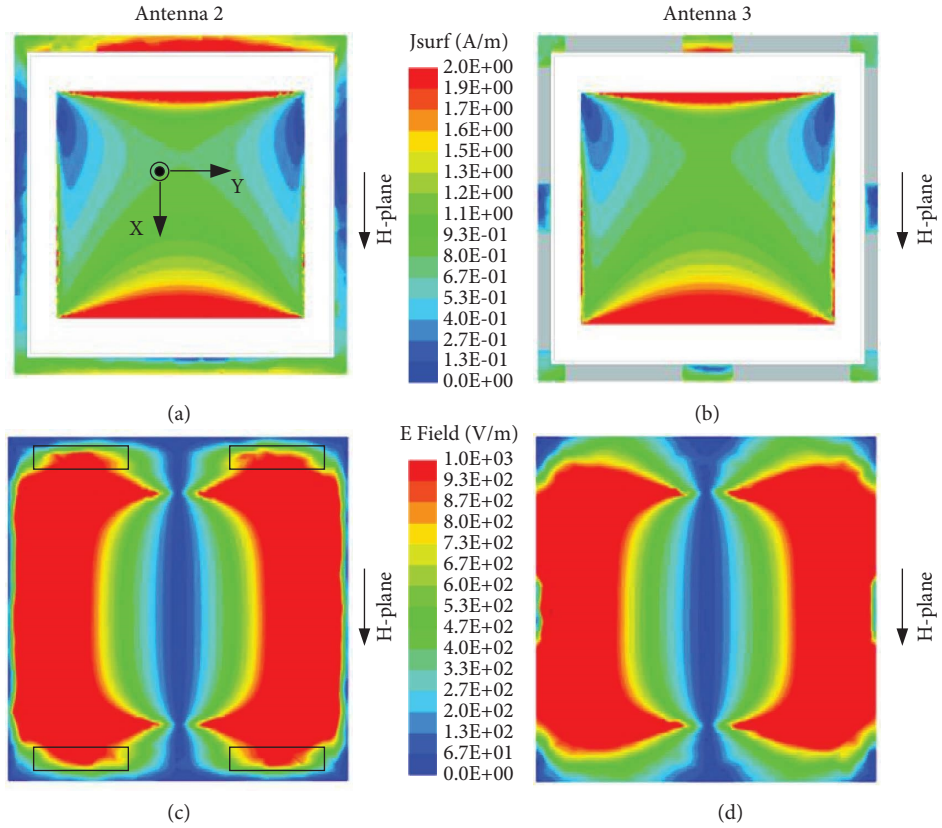

Figure 5: Surface current distributions of (a) antenna 2 and (b) antenna 3, and surface electric-field distributions of (c) antenna 2 and (d) antenna 3, when scanning at 60° in the *H*-plane at 1.7 GHz.

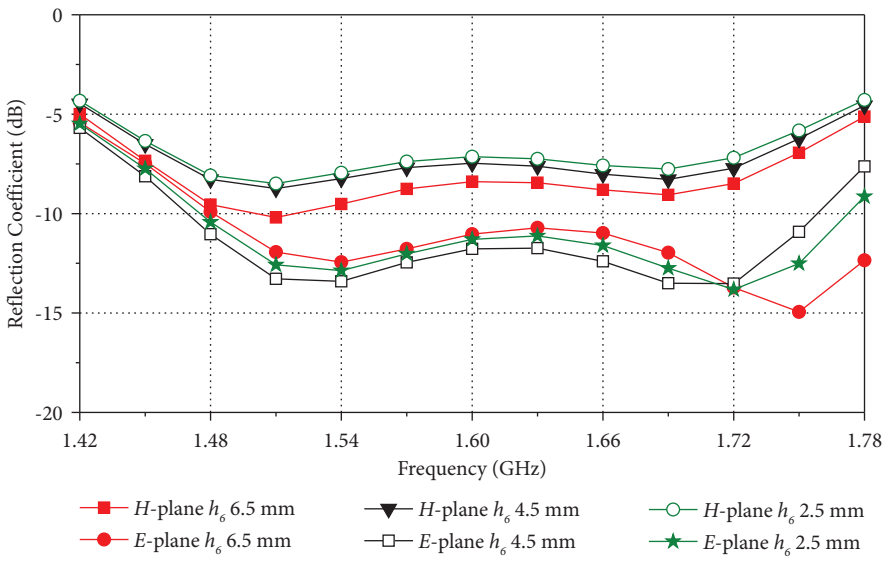

(a)

Figure 6: Continued.

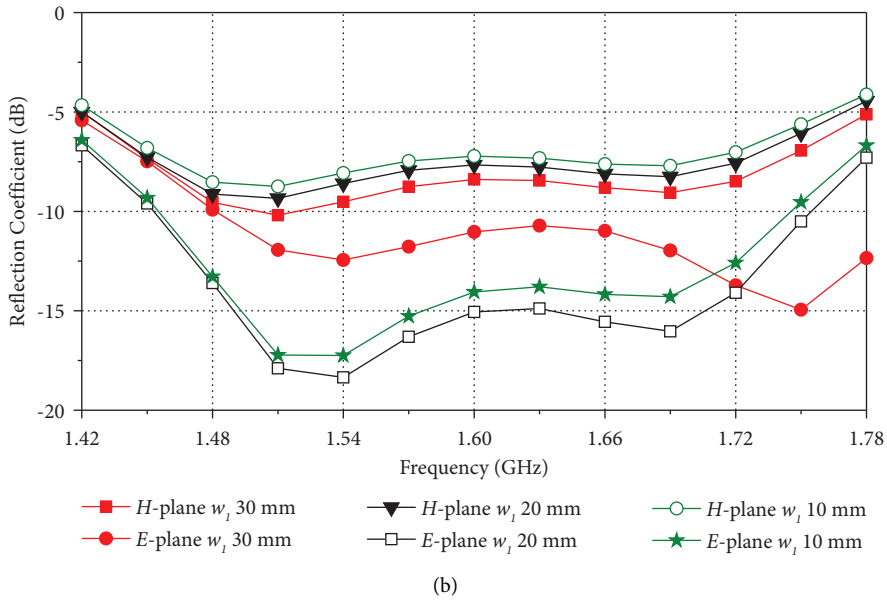

FIGURE 6: Parameter sweep analysis of (a) the depth h_6 and (b) the width w_1 of the wall notches.

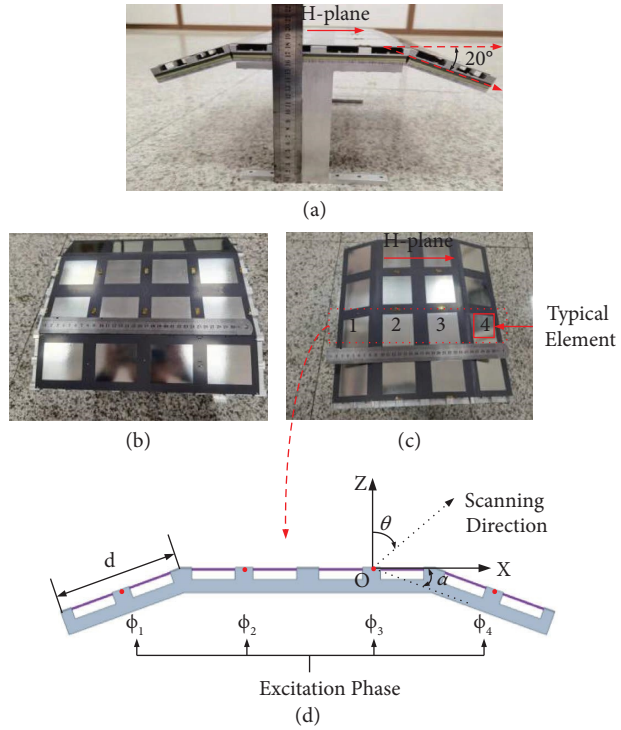

FIGURE 7: Prototype of the proposed 4 × 4 CPA. (a) Side view. (b, c) Top view. (d) Simplified schematic of the cross-section in the XOZ plane.

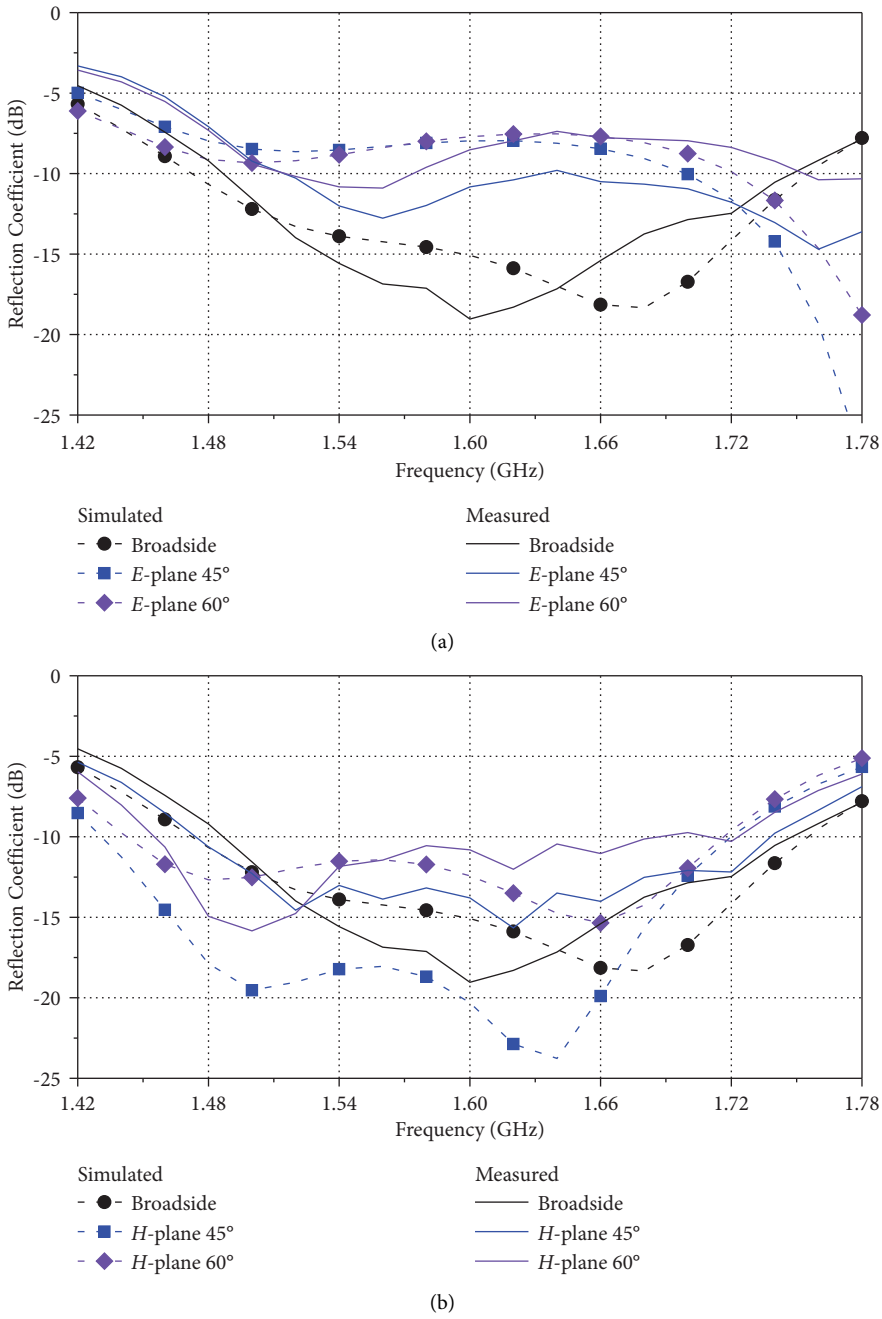

Figure 8: Measured and simulated active reflection coefficient of element 4 when scanning in the (a) *E*-plane and (b) *H*-plane.

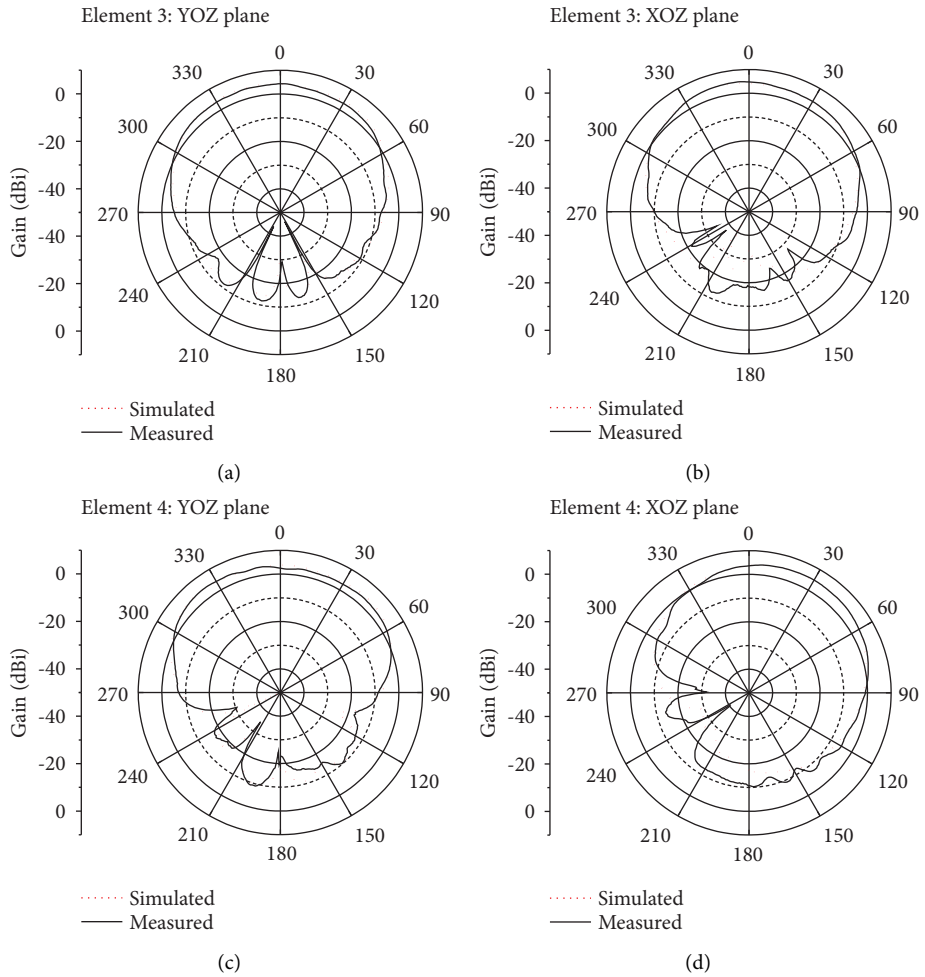

Figure 9: Measured and simulated element radiation patterns. Element 3 in (a) YOZ plane and (b) XOZ plane, and element 4 in (c) YOZ plane and (d) XOZ plane.

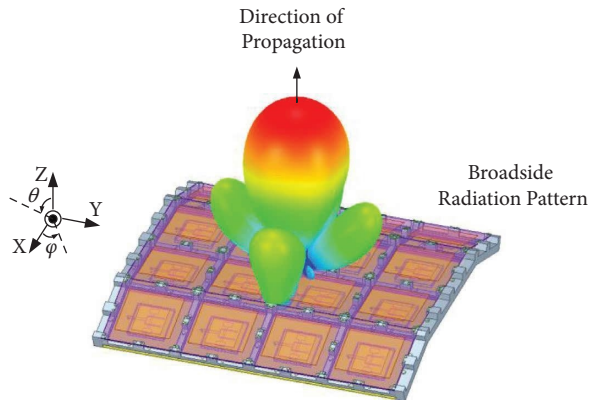

Figure 10: 3D radiation pattern of the 4 × 4 CPA at broadside radiation.

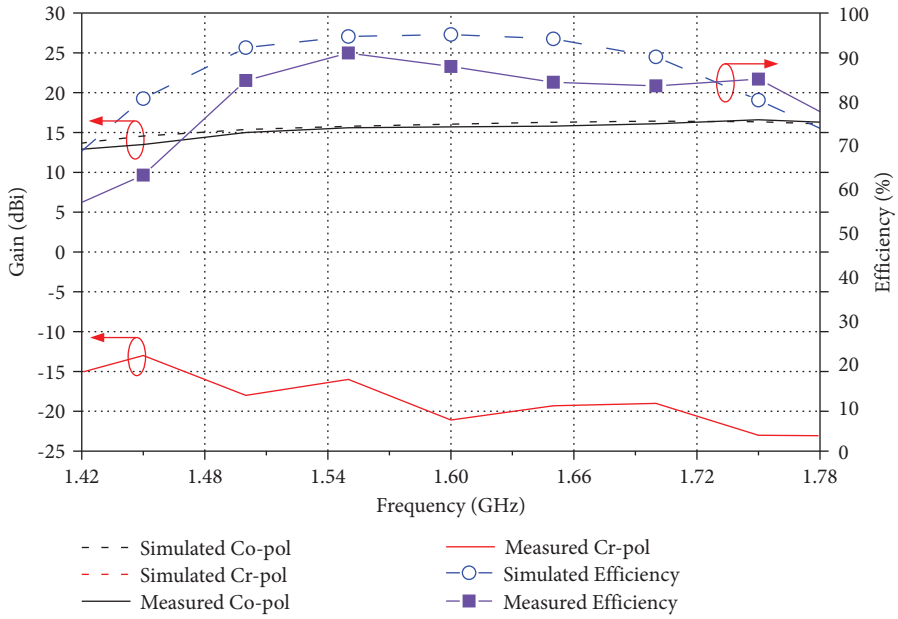

FIGURE 11: The co-polarized (co-pol) and cross-polarized (cr-pol) gains at broadside (left of the figure), and the efficiencies (right of the figure).

The element radiation patterns of elements 3 and 4 are shown in Figure 9. As can be seen, the measured element patterns agree well with the simulated results. Due to the bending of the edge elements, the radiation beams are offset from the Z-axis. Moreover, the 3D radiation pattern of the 4×4 CPA is shown in Figure 10. As a result of the overall symmetry of the array, the array beam points towards the Z-axis, i.e., the broadside radiation direction.

Figure 11 shows the measured copolarized (co-pol) and crosspolarized (cr-pol) gains and efficiencies of the array at broadside radiation, compared with the simulated results. As observed, the measured co-pol gain differs from the simulation by less than 1 dB across the entire band. The simulated cr-pol gain, being less than −60 dB, is not shown in the figure. However, the measured crosspolarization level is lower than −25 dB across the entire band, and falls below −30 dB in most of the band. This indicates that the array exhibits good isolation between co-pol and cr-pol radiations. Moreover, the measured efficiency exceeds 80% in most of the operating bands.

Figure 12 shows the measured and simulated normalized copolarized gain patterns when scanning in both the E-plane and H-plane at 1.7 GHz. As shown in the figure, the measured patterns reach an agreement with the simulated results, whether at broadside radiation or when scanning in the E/H-planes. The deviations between the peak-gain directions and the supposed scanning angles are attributable to the relatively small scale of the array prototype.

Moreover, a comparison between this work and previously reported patch arrays is presented in Table 1. Obviously, the proposed array features the largest scanning range. In terms of antenna profile, the conformal array in reference [20] has the lowest scanning range but at the cost of a narrower operating band and fixed-beam. As compared to other arrays, the proposed CPA features the advantages of both a low profile and wide-scanning performance, thereby making it suitable for conformal applications.

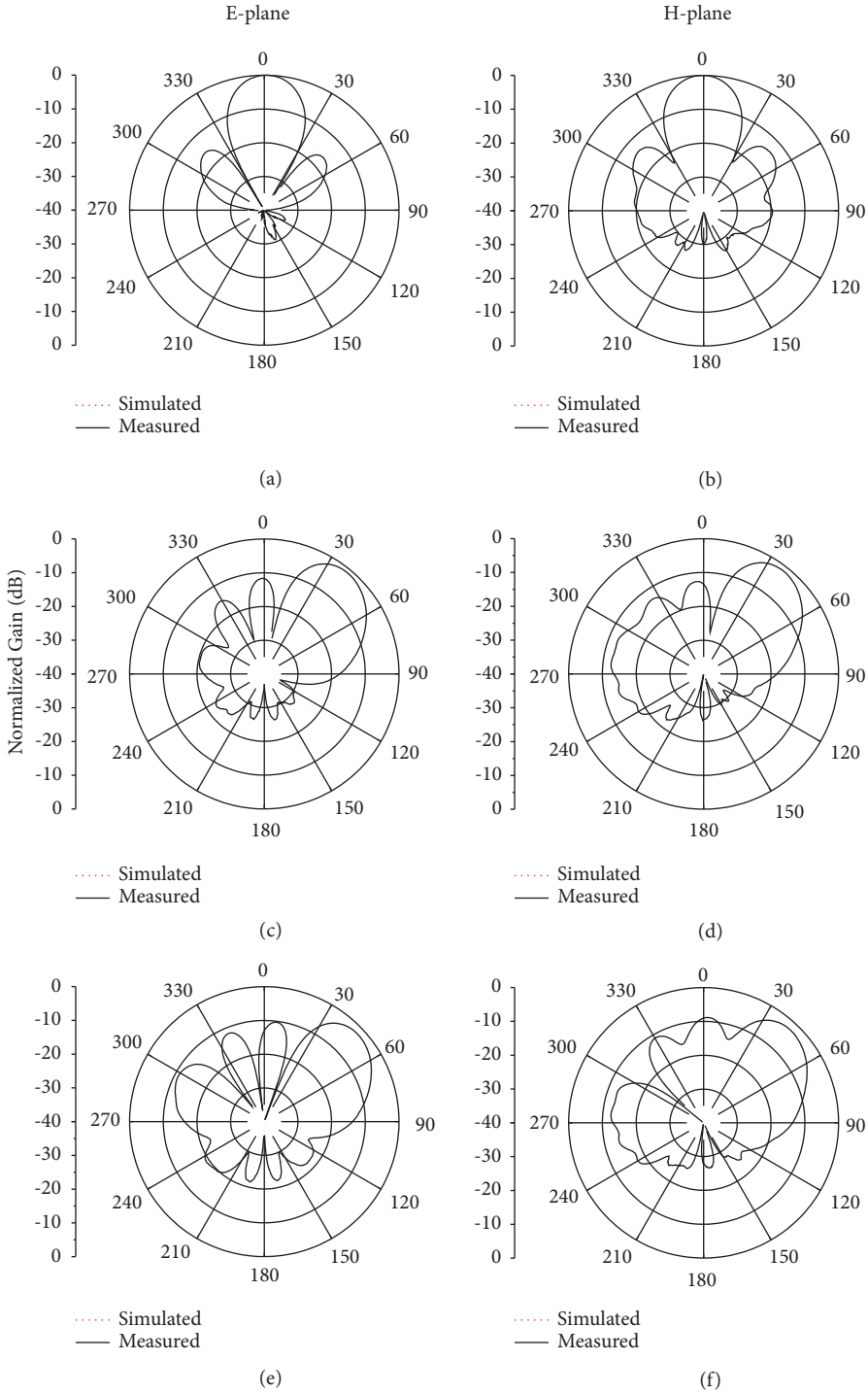

FIGURE 12: Measured and simulated normalized co-pol gain patterns of the 4 × 4 CPA prototype for various scan angles (0°, 45°, and 60°) in the *E*-plane and *H*-plane at 1.7 GHz.

Table 1: Comparison between this work and related works.

Ref	Operating band (GHz)	Profile	Scan range in E/H-planes	Type of array
[25]	2.7–2.9 (7%)	0.077 λ_h	±45°/±45°	Planar phased array
[20]	2.45–2.55 (4%)	0.004 λ_h	0°/0°	Conformal array
[21]	8.5–11.5 (27%)	0.168 λ_h	N. A	Conformal array
[26]	9.5–10 (5%)	0.021 λ_h	N. A	Conformal series-fed array
This work	1.45–1.75 (18.75%)	0.086 λ_h	±60°/±60°	CPA

4. Conclusion

A low-profile wide-scanning conformal phased array operating in 1.45~1.75 GHz is proposed in this paper. To obtain a better impedance matching, a backed cavity is employed, partially filled with high-permittivity dielectric to reduce the antenna profile. Additionally, the cavity side walls are extended to enhance interelement isolation, and parts of the side walls that support the strong coupling currents are cut to further improve scanning performance. Consequently, the designed element features a low profile of 0.086 λ_h, while achieving a relatively large fractional bandwidth of 18.75% when scanning at ±60° in the E-plane and H-plane. Lastly, the wide-scanning ability of the CPA is experimentally verified by a 4×4 CPA prototype, demonstrating the effectiveness of the design method.

Data Availability

The data used to support the findings of this study are included within the article.

Conflicts of Interest

The authors declare that they have no conflicts of interest.

Acknowledgments

This work was supported by the Natural Science Foundation of China Projects under Grants U20A20165 and 61721001.

References

[1] J. J. M. de Wit, A. Meta, and P. Hoogeboom, "Modified range-Doppler processing for FM-CW synthetic aperture radar," *IEEE Geoscience and Remote Sensing Letters*, vol. 3, no. 1, pp. 83–87, 2006.

[2] A. M. Horne and G. Yates, "Bistatic synthetic aperture radar," *RADAR 2002*, pp. 6–10, Edinburgh, UK, 2002.

[3] H. Du and J. Wang, "A broadband millimeter wave fixed-beam leaky-wave antenna with stable broadside radiation," *The Applied Computational Electromagnetics Society: ACES*, pp. 1–3, 2023.

[4] I. L. Vilenko, A. K. Tobolev, A. V. Shishlov, Y. V. Krivosheev, M. S. Uhm, and S. H. Yun, "Millimeter wave reflector antenna with wide angle mechanical beam scanning," in *Proceedings of the 2021 International Conference Engineering and Telecommunication (En&T)*, pp. 1–4, Dolgoprudny, Russian Federation, November 2021.

[5] W.-Q. Wang and H.-Z. Shao, "A flexible phased-MIMO arrayantenna with transmit beamforming," *International Journal of Antennas and Propagation*, vol. 2012, Article ID 609598, 10 pages, 2012.

[6] M. M. Islam, M. Leino, R. Luomaniemi et al., "E-band beam-steerable and scalable phased antenna array for 5G access point," *International Journal of Antennas and Propagation*, vol. 2018, Article ID 4267053, 10 pages, 2018.

[7] L.-Z. Song, X. Wang, and P.-Y. Qin, "Single-feed multibeam conformal transmitarrays with phase and amplitude modulations," *IEEE Antennas and Wireless Propagation Letters*, vol. 21, no. 8, pp. 1669–1673, 2022.

[8] D. Sun, R. Shen, and X. Yan, "A broadband conformal phased array antenna on spherical surface," *International Journal of Antennas and Propagation*, vol. 2014, Article ID 206736, 5 pages, 2014.

[9] R. J. Mailloux, *Phased Array Antenna Handbook*, Artech House, Boston, MA, USA, 2005.

[10] Z. Wei and Y. Junfeng, "A design of vertical polarized conformal antenna and its array based on UAV structure," *International Journal of Antennas and Propagation*, vol. 2017, Article ID 9769815, 12 pages, 2017.

[11] S. Wang, F. Jiang, J. Chen, and W. Pan, "A conformal log-period foldedslot antenna with reduced size," in *Proceedings of the 2013 IEEE Antennas and Propagation Society International Symposium (APSURSI)*, pp. 890-891, Orlando, FL, USA, July 2013.

[12] Z. Li, K. Wang, Y. Lv, S. Qian, X. Zhang, and X. Cui, "Wing conformal load-bearing endfire phased array antenna skin technology," *IEEE Transactions on Antennas and Propagation*, vol. 71, no. 3, pp. 2064–2069, 2023.

[13] J. Mittermayer, A. Moreira, and O. Loffeld, "Spotlight SAR data processing using the frequency scaling algorithm," *IEEE Transactions on Geoscience and Remote Sensing*, vol. 37, no. 5, pp. 2198–2214, 1999.

[14] H. R. Khaleel, H. M. Al-Rizzo, D. G. Rucker, and S. Mohan, "A compact polyimide-based UWB antenna for flexible electronics," *IEEE Antennas and Wireless Propagation Letters*, vol. 11, no. 8, pp. 564–567, 2012.

[15] J.-J. Peng, S.-W. Qu, M. Xia, and S. Yang, "Wide-scanning conformal phased array antenna for UAV radar based on polyimide film," *IEEE Antennas and Wireless Propagation Letters*, vol. 19, no. 9, pp. 1581–1585, 2020.

[16] F.-P. Lai, L.-W. Chang, and Y.-S. Chen, "Miniature dual-band substrate integrated waveguide slotted antenna array for

millimeter-wave 5G applications," *International Journal of Antennas and Propagation*, vol. 2020, Article ID 6478272, 10 pages, 2020.

[17] Y. Liu, H. Yang, Z. Jin, F. Zhao, and J. Zhu, "A multibeam cylindrically conformal slot array antenna based on a modified rotman lens," *IEEE Transactions on Antennas and Propagation*, vol. 66, no. 7, pp. 3441–3452, 2018.

[18] O. Bayraktar and O. A. Civi, "Circumferential traveling wave slot array on cylindrical substrate integrated waveguide (CSIW)," *IEEE Transactions on Antennas and Propagation*, vol. 62, no. 7, pp. 3557–3566, 2014.

[19] J.-J. Peng, S.-W. Qu, M. Xia, and S. Yang, "Conformal phased array antenna for unmanned aerial vehicle with ±70° scanning range," *IEEE Transactions on Antennas and Propagation*, vol. 69, no. 8, pp. 4580–4587, 2021.

[20] B. D. Braaten, S. Roy, I. Irfanullah, S. Nariyal, and D. E. Anagnostou, "Phase-compensated conformal antennas for changing spherical surfaces," *IEEE Transactions on Antennas and Propagation*, vol. 62, no. 4, pp. 1880–1887, 2014.

[21] D. Sun, W. Dou, and L. You, "Application of novel cavity-backed proximity-coupled microstrip patch antenna to design broadband conformal phased array," *IEEE Antennas and Wireless Propagation Letters*, vol. 9, pp. 1010–1013, 2010.

[22] Y. Xia, B. Muneer, and Q. Zhu, "Design of a full solid angle scanning cylindrical-and-conical phased array antennas," *IEEE Transactions on Antennas and Propagation*, vol. 65, no. 9, pp. 4645–4655, 2017.

[23] H. C. Mao, S. W. Qu, and S. Yang, "Edge Truncation Effect Suppression of Phased Cavity-Backed Stacked Patch Array," *IEEE Antennas and Wireless Propagation Letters*, vol. 99, 2023.

[24] S. Yu, N. Kou, J. Jiang, Z. Ding, and Z. Zhang, "Beam steering of orbital angular momentum vortex waves with spherical conformal array," *IEEE Antennas and Wireless Propagation Letters*, vol. 20, no. 7, pp. 1244–1248, 2021.

[25] H. Saeidi-Manesh and G. Zhang, "High-isolation, low cross-polarization, dual- polarization, hybrid feed microstrip patch array antenna for MPAR application," *IEEE Transactions on Antennas and Propagation*, vol. 66, no. 5, pp. 2326–2332, 2018.

[26] S. Ogurtsov and S. Koziel, "A conformal circularly polarized series-fed microstrip antenna array design," *IEEE Transactions on Antennas and Propagation*, vol. 68, no. 2, pp. 873–881, 2020.